ISSN (Print) 1226-1750
ISSN (Online) 2233-6656
Journal of Magnetics 27(3), 303-308 (2022) https://doi.org/10.4283/JMAG.2022.27.3.303

Synthesis and Magnetic Properties of FeCo Alloy Nanowires via AC Frequency Conversion Electrodeposition

Lirong Wang[1,2], Shunzhen Feng[1,3], Tingting Lu[1], Lizhen Zhen[1], Jiwei Zhang[1], and Lihu Liu[1]*

[1]*College of Physics, Hebei Normal University, Shijiazhuang 050024, China*
[2]*College of Chengde Radio Television, Chengde 067000, China*
[3]*College of Shijiazhuang, Shijiazhuang 050035, China*

(Received 18 March 2022, Received in final form 14 August 2022, Accepted 22 August 2022)

Binary alloy nanowires of Fe_3Co_7 system are synthesized in the highly ordered porous anodic aluminum oxide (PAA) templates by AC frequency (5, 50, 120, and 200 Hz) conversion electrodeposition method. High resolution field emission transmission electron microscope (HRTEM) and Lorenz TEM (LTEM) were used to study the morphology and the magnetic domain structure of the Fe_3Co_7 alloy nanowires, respectively. Magnetic measurements showed that the M-H curves presented a discontinuity in a restricted magnetic field, but with high squareness (about 90 %). Quantitative local measurements of the magnetic properties of the nanowires are explored by differential phase contrast (DPC) imaging. The magnetic properties, however, were significantly affected by the AC frequency, which is correlated with the specific magnetic structure formation of Bloch line. We reported herein a detailed investigation on Fe_3Co_7 alloy nanowires and their magnetic properties.

Keywords : nanowires, electrodeposition, magnetic property, Lorenz

1. Introduction

One-dimensional nanostructure materials such as nanowires, nanorods, and nanotubes play a special role in the field of nanoscience and nanotechnology due to their distinctive properties and potential applications [1-3]. In these materials, ferromagnetic nanostructures had gained a lot of attention of scientific community in the last few years due to their potential applications in the fields of ultra-high density magnetic storage and microsensors [4, 5]. One simple and economical way to achieve nanomagnetic arrays over a large area is based on highly ordered PAA templates [6]. Electrochemical deposition is a simple, efficient, and versatile technique. Until now, three different kinds of electrochemical deposition methods are applied for filling the pores of PAA template: direct current (DC) electrodeposition [7], pulse electrodeposition (PED) [8], and alternating current (AC) electrodeposition [9]. Filling of PAA pores with metallic or magnetic nanowires via DC or PED electrodeposition is a tedious process and requires many steps. Previously our group had reported the formation of Ni-Zn alloy nanowire by DC electrodeposition mode using PAA templates as the matrix material [10]. In contrast, AC electrodeposition has been proved a very powerful technique and it does not need the detachment of PAA template from the Al-substrate or modification of the barrier layer. Moreover, the Al-substrate can be used as cathode during the metal ions electrodeposition process.

Due to the high aspect ratio, nanoscale cylindrical FeCo NW arrays present obvious shape anisotropy, which can enhance the coercivity of it and make it a good choice as perpendicular magnetic recording media [11]. In this regard, we described an alternative pathway for preparation of FeCo binary alloy nanowires using AC frequency conversion electrodeposition, and the AC frequency was regulated to 5, 50, 120, and 200 Hz, respectively. Starting from a well-distributed structure, a subsequent frequency increase resulted in different structural FeCo alloy nanowires. These FeCo nanowires, synthesized by AC frequency conversion electrodeposition, exhibit significant differences in their magnetic properties compared with that of typical FeCo nanowires [12]. In the family of FeCo alloy NWs, many efforts have been made to research the magnetization reversal process through major hysteresis loops (M-H curves) [13]. However, an unconventional magnetic

*Corresponding author: Tel: +86-311-80787300
Fax: +86-311-80789790, e-mail: lihuliut@126.com

phenomenon, i.e. a discontinuous hysteresis loop can be obtained and the origin of which will be analyzed in this paper. In our opinion, the M-H curves discontinuity may be due to the existence of specific magnetic domain defects, which may influence the magnetization reversal process, in the FeCo nanowires. As suggested by the superconducting quantum interference device (SQUID) and magnetic differential phase contrast (DPC) model results, Bloch lines formation was indeed found during magnetization of the FeCo nanowires. Our findings not only provide a new method to synthesize alloy nanowires but also open the door to modulating magnetic properties of alloy nanowires by controlling the ferromagnetism structure for future magnetic applications.

2. Experiments

The porous anodic alumina (PAA) templates used to deposit FeCo nanowires in the present work were prepared by high-purity (99.99 %) Al strips as the starting material. Before anodization, Al strips were annealed at 500 °C for 2 h in Ar to remove the mechanical stresses. Subsequently, the strips were cut into circular pieces with diameter of 1 cm to be electropolished in a solution of perchloric acid and ethanol (1:4) at room temperature, followed by rinsing in deionized water many times and drying by hyperbaric Ar. A two-electrode system, with the well cut Al piece as a working electrode and graphite sheet (5 cm × 2 cm) as a counter electrode, was used for electrochemical anodization. Anodization was conducted in 0.3 M aqueous oxalic acid electrolyte at constant voltage of 40 V for 1 h using a DC power source at 5 °C. Subsequently, a nonequilibrium anodization process was employed to reduce the barrier layer [14]. The voltage was lowered by 3 V/min until 10 V was reached, and then holding the voltage at 10 V for 3 min to equilibrate the barrier layer, thus facilitating the next electrodeposition of the metals.

To deposit FeCo alloy nanowires in PAA templates, the AC electrodeposition technique was performed in a simple electrochemical cell consisting of two electrodes: the PAA template with Al base and a square platinum foil were used as working and counter electrode, respectively. The FeCo alloy nanowires were then electrodeposited in the synthesized PAA template in an electrolyte of the following composition: $FeSO_4 \cdot 7H_2O$ 29 g/l; $CoSO_4 \cdot 7H_2O$ 40 g/l; boric acid 40 g/l and Ac acid 0.8 g/l for the final alloy nanowires. The electrodeposition was carried out at room temperature with an AC voltage of 16 V_{rms} in various frequency and deposition time of 15 min. The AC frequency was set at 5, 50, 120, and 200 Hz, respectively. All electrochemical measurements were performed using an AC frequency converter power supply (PCL 500E, Japan) controlled by a PC.

The phase composition of FeCo alloy nanowires with PAA template was investigated by XRD using a Philips X'Pert-MPD x-ray diffractometer (Cu K_α radiation, 40 kV, 40 mA). Then a size of 3 mm × 6 mm rectangle was cut from the as-deposited samples for subsequent SQUID and scanning TEM (STEM, FEI) analysis after removal of the membranes. The chemical compositions of the nanowires were examined through energy dispersive spectroscopy (EDS) attached with TEM system.

3. Results and Discussion

Figure 1(a) shows cross-sectional SEM image of the PAA template and Fig. 1(b) presents a responsive STEM mode image of the nanowire. It may be seen that the nanowire is not smooth and with average diameter about 47 nm, which corresponds to the pore structure of the PAA template (Fig. 1(a)). To resolve elemental distribution, elemental mapping was conducted to identify the distribution of Fe and Co ions in the nanowire. The elemental-mapping analysis (Fig. 1(c) and Fig. 1(d)) illustrates the uniform spatial distribution of Fe and Co. Given the chemical compositions, which can be analyzed by EDX, and the accurate compositions of the Fe-Co alloy nanowire products are determined to be Fe:Co= 24:76. The quantitative analysis obtained from EDX characterization is considered close to the concentration ratio of the metallic compounds Fe_3Co_7, and which can be proved by the next XRD analyzation. However, there is an obvious difference in the distribution range of element

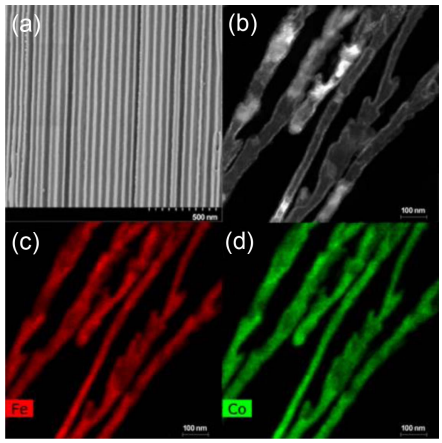

Fig. 1. (Color online) (a) Cross-sectional SEM image of the PAA template; (b) HADDF-STEM image of an individual FeCo alloy nanowire; and the corresponding elemental maps (c) Fe, and (d) Co of the as-synthesized FeCo nanowires.

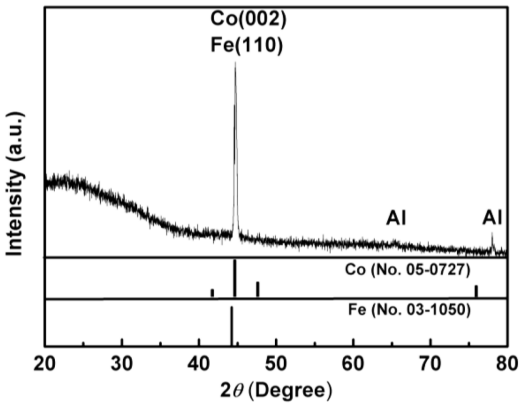

Fig. 2. XRD patterns of the as-synthesized FeCo nanowires. The peaks correspond to Fe_7Co_3 and Al phases with crystalline structure.

which can be viewed in the elemental-mapping result. According to the growth mechanism of 1-*d* metallic nanomaterials by method of template-based electrodeposition [15], in the low frequency deposition, metallic cations have enough time to diffuse and move directly to the cathode and are reduced. This growth process is favorable to drive the FeCo nanowires growing from the bottom to the top and form a uniform microstructure. On the contrary, in the process of high frequency deposition, both metallic cations of Co^{2+} and Fe^{2+} are inclined to move to the PAA template pore walls and deoxidized there. It is worth noting that, although growing in the same mode, hexagonal close-packed (*hcp*) cobalt with close-packed structure prefers to form tube while body-centered-cubic (*bcc*) iron form wire. In our previous work [16], we found that cobalt tend to grow along the kinetics crystallographic plane and form tube-like structure with kinetics controlling the deposition process.

The X-ray diffraction (XRD) analysis gives the crystal phase and accurate composition of these nanowires. As shown in Fig. 2, there is an overlap of *hcp* <002> Co and *bcc* <110> Fe peaks observed in the XRD pattern (JCPDS No. 05-0727 and 03-1050) because they lie close to each other. Moreover, no peaks corresponding to pure Co or Fe have been observed in the XRD patterns, indicating the formation of an alloy phase. This result has been further verified from the binary phase diagram of Co-Fe. A mixed structure of *hcp* and *bcc* phases has been observed in the binary phase diagram of Co-Fe at $Co_{76}Fe_{24}$ alloy composition. Since the XRD measurements were performed without removing the alumina template, a broad dispersion peak in lower angle region (20° to 38°) should mainly ascribe to the amorphous PAA template, one can also observe Al peaks ($2\theta = 65.2°$ and 78.3°) that are sharp in the XRD profiles besides.

The magnetic properties of Fe-Co alloy nanowires embedded in PAA template are closely related to their microstructure. To observe the magnetic properties, the materials were evaluated with field sweep from -10 to 10 kOe at 300 K using magnetic property measurement

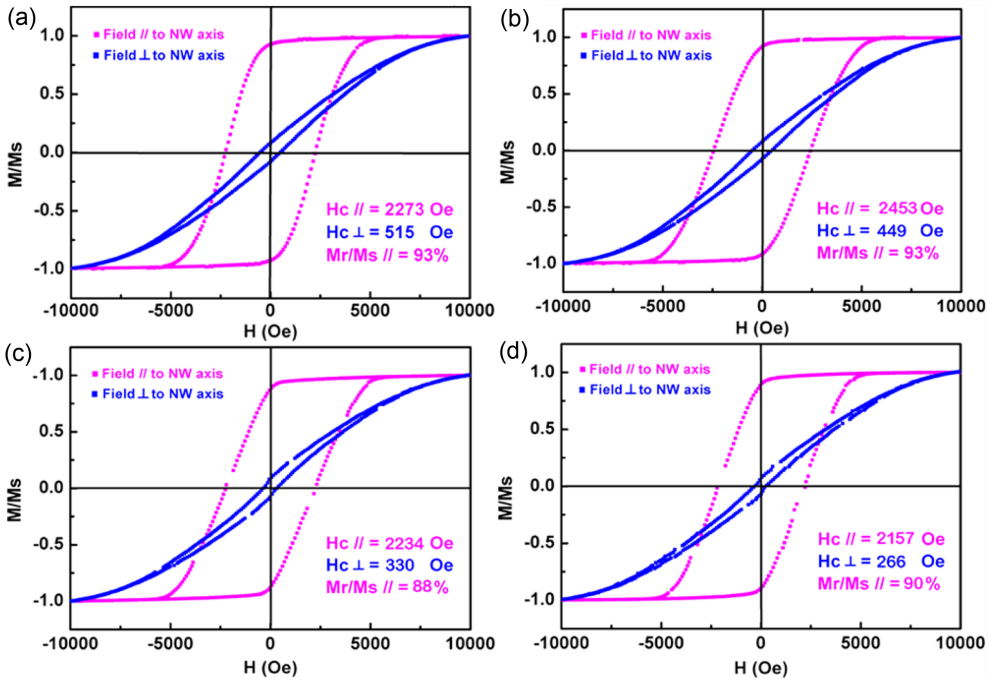

Fig. 3. (Color online) Magnetization curves in both parallel and perpendicular directions of magnetic field with respect to the nanowire axis: (a) 5 Hz, (b) 50 Hz, (c) 120 Hz, and (d) 200 Hz.

system (MPMS, Quantum Design). Fig. 3 shows the hysteresis loops obtained from FeCo nanowire samples with the external magnetic field applied perpendicular (⊥) to the sample plane (parallel to the wire axis) and parallel (//) to the sample plane (perpendicular to the wire axis), respectively. These hysteresis loops reveal that all the alloy arrays exhibit uniaxial magnetic anisotropy, with the easy axis parallel to the longitudinal axis direction of nanowires. Taking into account the big aspect ratio of the alloy nanowires and the preferential orientation of the samples exhibited in the XRD result (<002> of Co is the easy-magnetization axis of which), we expect the uniaxial anisotropy to originate from both shape and magneto-crystalline anisotropy. In view of the obvious uniaxial magnetic anisotropy of the samples, according to the Stoner-Wohlfarth model [17], the theoretical coercivity (Hc) values for the alloy nanowires with magnetic field parallel to the wire axis can be calculated, as shown in Fig. 4. It can be seen from the analytical calculation that the magnetization reversal is better fitted to the experimental data. The variance between experimental values and theoretical ones may be regarded as the result of a simple rotation model. After all, the shape of our alloy nanowires is different with nanoparticles. It should be noted that buckling model is dominative but not coherent rotation in the columnar material, which will cause smaller coercivity.

From Fig. 4, one can observe that the coercivity values firstly increase with the increase of frequency and then decrease with further increase of frequency. However, the maximum coercivity value here is about 23 % smaller than the one found in previous studies on Co-Fe nanowires [18]. For fields normal to the wires, the coercivities decrease monotonously from 515 to 266 Oe. On the other hand, the squareness (SQ = M_r/M_s) of all samples, as list in Fig. 3, does not change a lot and maintains at a very high level (at least 88 %), which indicates it may play an important role in the realm of magnetic recording. Interestingly, for the samples synthesized at high frequency, one can observe that there are obvious discontinuous intervals in the M-H curves (as shown in Fig. 3(c) and 3(d)). Furthermore, four intervals can be seen in each hysteresis loop, and it seemed that they symmetrically distribute relative to the origin in pairs.

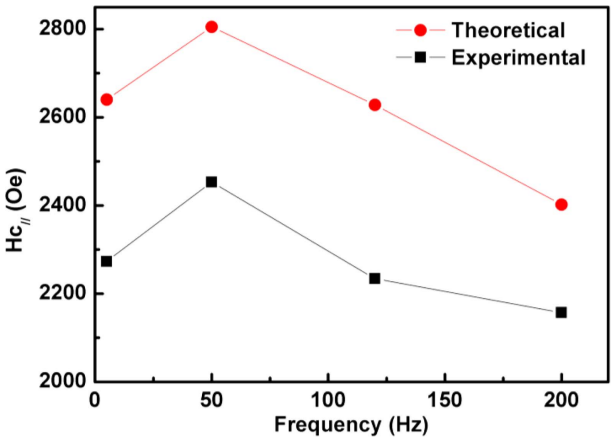

Fig. 4. (Color online) Experimental and calculated coercivity (Hc) of aligned FeCo alloy NWs. The red solid dots corresponds to the analytical plot calculated by using adapted Stoner-Wohlfarth model and black dots correspond to the experimental values with external field parallel to the wire axis.

Figure 5 showed the enlarged view of the hysteresis loop in the first quadrant of the sample synthesized at AC frequency of 200 Hz, and which was obtained with the applied field parallel to the long axis of the nanowires. From Fig. 5, there is a discontinuous interval from Hr_1 (3237 Oe) to Hr_2 (3591 Oe) can be seen in the hysteresis loop, over which ($Hr_1 < H < Hr_2$) there is no magnetic moment can be detected in this reversal process, which is actually different with the common Barkhausen jump [19]. Once H increases to Hr_2, the hysteresis loop keep continuous again by magnetization jump process. So we think there must be particular magnetic structures arise in the nanowires. Similar phenomena had been reported by many groups and which could be attributed to different reasons [20, 21]. Among them, the appearance of Bloch line is considered to be an important factor. As we know, the functionality of a Bloch line is that it can change the original magnetic structure of the sample and then affect the reversal of magnetic moment. According to the theory

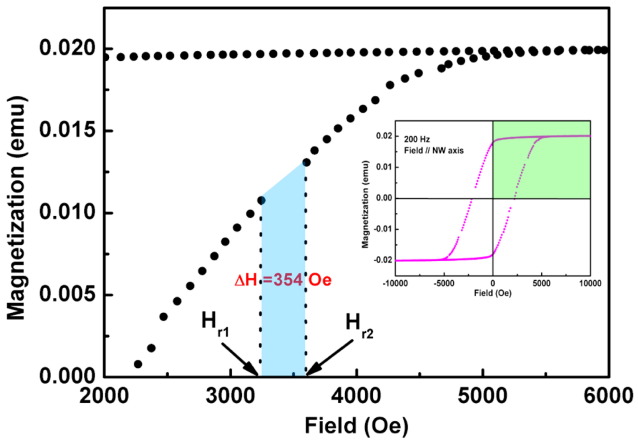

Fig. 5. (Color online) The enlargement of the hysteresis loop in the first quadrant of the sample synthesized at AC frequency of 200 Hz. Inset chart illustrates the original graph of this figure.

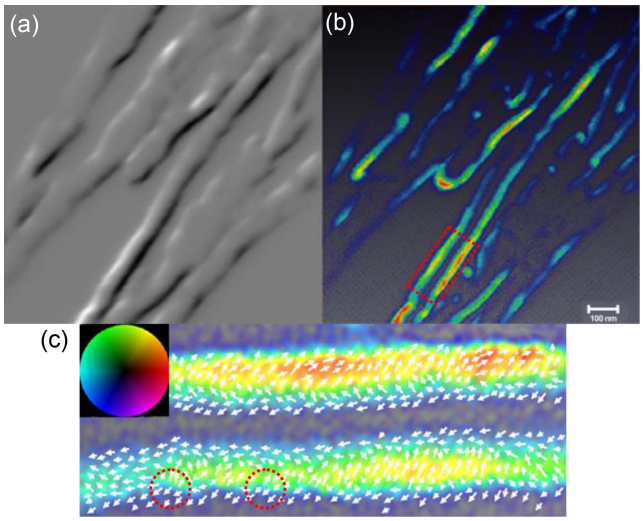

Fig. 6. (Color online) (a) DPC image of FeCo alloy nanowires synthesized at AC frequency of 200 Hz; and (b) color-coded magnetic map according to (a); (c) is schematic diagram of magnetic flux configurations and forming of Bloch lines (enclosed with red dotted circles) in the enlarged image corresponding to the area surrounded by red dotted rectangle in (b). The color wheel represents the magnetization direction.

of Bloch line [22], we calculate the saturation magnetization value Ms = 4.38 × 10^2 emu/cm^3 for the sample synthesized with AC frequency of 200 Hz. In all calculations, considering the filling ratio of the PAA template, the average values of the length and diameter of the wires were adopted to get the result. Through comparisons, we obtained that 8Ms = 3504 ≈ Hr_2. This suggests that a vertical Bloch line may exist in the FeCo alloy nanowires here and which can be responsible for the magnetization jump in the present samples. Additionally in the heterogeneous nanowires with strong magnetic anisotropy, due to the existence of the structural defects, which may conduce to the formation of the local inhomogeneities, i.e. Bloch lines, too.

As demonstrated above, the electrodeposition process was carried out under a constant voltage (16 V_{rms}) but with different frequency. Thus, such a different frequency would give rise to the different microstructural nanowires can be estimated. So, we can conclude that the magnetic properties are related to the microstructure of the samples.

In the present study, we employed an alternative technique to investigate the possible causes that lead to the discontinuous intervals by way of differential phase contrast (DPC), which is one of the techniques of LTEM that enables analysis of local magnetic properties and offers a powerful approach for characterizing magnetic microstructure [23-25]. Fig. 6(a) shows the standard static DPC image of the FeCo alloy nanowires synthesized at 200 Hz. The DPC induction map indicates that the nanowire possesses an inhomogeneous structure, which can be strikingly represented in a color-coded magnetic map (Fig. 6(b)). The colored map shows the direction of magnetization in the nanowires, and the color saturation encodes the magnetization magnitude. It can be seen that the color saturation is lower in the central portion than the outer layer of the nanowire, which reveals that there is stronger magnetic moment exists at the outer layer of the nanowire. Thus, it is reasonably considered that irregular distributions of colors may result from the inhomogeneous magnetization distribution and well correspond to the properties of the nanowires, i.e., high remanence and large coercivity.

According to the color-coded magnetic map, we can conclude that the distribution of magnetic fluxes takes on the clockwise (CW) or counterclockwise (CCW) mode in the nanowires [26]. It can be deduced that an abnormal line will be formed when the CW and CCW magnetic fluxes encounter. In Fig. 6(c), a schematic diagram of magnetic fluxes configurations was drawn, and it could be found Bloch lines (enclosed with red dotted circles) were formed in the boundary of magnetic domain, which is considered the main reason to cause the discontinuous intervals and plays an important role in the magnetization reversal process.

4. Conclusions

In this study, Fe-Co alloy nanowires were obtained by AC electrodeposition method. The electrodeposition was carried out at room temperature with an AC voltage of 16 Vrms and the AC frequency was set at 5, 50, 120, and 200 Hz, respectively. For the sample prepared at 200 Hz, which showed a high squareness (93 %) and saturation magnetization value Ms = 4.38 × 10^2 emu/cm^3. There are obvious discontinuous intervals in the M-H curves can be observed in the samples synthesized at high frequency. Firstly, the microstructure creates conditions for the existence of magnetic flux in clockwise or counterclockwise mode. Secondly, the co-existence and encounter of the CCW and CW chirality magnetic flux will bring to Bloch line in the magnetic domain structure, which can be explored by using DPC magnetic imaging technique and is consider to be the intrinsic reason for the discontinuous intervals in the process of magnetization reversal.

Acknowledgement

This work is supported by the Science and Technology

Project of Hebei Education Department (Grant No. QN2021088 and 19k97635D) and the Natural Science Foundation of Hebei Province (Grant No. A2020205038).

References

[1] B. Bari, J. H. Lee, T. Jang, P. Won, S. H. Ko, K. Alamgir, M. Arshad, and L. J. Guo, J. Mater. Chem. A **4**, 11365 (2016).
[2] M. Aslam, R. Bhobe, N. Alem, S. Donthu, and V. P. Dravid, J. Appl. Phys. **98**, 074311 (2005).
[3] Jinglei Yang, Xiaoping Shen, Guoxing Zhu, Zhenyuan Ji, and Hu Zhou, RSC Adv. **4**, 386 (2014).
[4] Debanjan Bhowmik, Mark E. Nowakowski, LongYou, OukJae Lee, David Keating, Mark Wong, Jeffrey Bokor, and Sayeef Salahuddin, Sci. Rep. **5**, 11823 (2015).
[5] Palanisamy Kannan, Thandavarayan Maiyalagan, Enrico Marsili, Srabanti Ghosh, Joanna Niedziolka-Jönsson, and Martin Jönsson-Niedziolk, Nanoscale **8**, 843 (2016).
[6] Dongdong Li, Richard S. Thompson, Gerd Bergmann, and Jia G. Lu, Adv. Mater. **20**, 4575 (2008).
[7] P. S. Fodor, G. M. Tsoi, and L. E. Wenger, J. Appl. Phys. **91**, 8186 (2002).
[8] Oana Dragos, Horia Chiriac, Nicoleta Lupu, Marian Grigoras, and Ibro Tabakovic, J. Electrochem. Soc. **163**, D83 (2016).
[9] Ghafar Ali and Muhammad Maqbool, Nanoscale. Res. Lett. **8**, 352 (2013).
[10] Lihu Liu, HaitaoLi, Shenghua Fan, and Jianjun Gu, J. Magn. Magn. Mater. **321**, 3511 (2009).
[11] C. L. Londono-Calderón, A. Londono-Calderón, O. Moscoso-Londono, A. Galindo, A. Ponce, L. G. Pampillo, R. Martínez-García, M. J. Yacamán, and M. Knobel, Phys. Status Solidi A **219**, 2100265 (2022).
[12] D. H. Qin, L. Cao, Q. Y. Sun, Y. Huang, and H. L. Li, Chem. Phys. Lett. **358**, 484 (2002).
[13] E. Paimozd, O. Mirzaee, and M. Tajally, J. Magn. Magn. Mater. **523**, 167582 (2021).
[14] R. C. Furneaux, W. R. Rigby, and A. P. Davidson, Nature **337**, 147 (1989).
[15] S. Thongmee, H. L. Pang, J. Ding, and J. Y. Lin, J. Magn. Magn. Mater. **321**, 2712 (2009).
[16] Huimin Zhang, Xiuli Zhang, Jingjing Zhang, Ziyue Li, and Huiyuan Sun, J. Electrochem. Soc. **160**, D41 (2013).
[17] E. C. Stoner and E. P. Wohlfarth, Philos. Trans. R. Soc. Lond. A **240**, 599 (1984).
[18] K. I. Arai, H. W. Kang, and K. Ishiyama, IEEE Trans. Magn. **27**, 4906 (1991).
[19] D. Salazar-Aravena, J. Escrig, and D. Laroze, J. Magn. Magn. Mater. **497**, 165935 (2020).
[20] N. Viart, R. Sayed Hassan, J. L. Loison, G. Versini, F. Huber, P. Panissod, C. Meny, and G. Pourroy, J. Magn. Magn. Mater. **279**, 21 (2004).
[21] Q. K. Ong, A. Wei, and X. M. Lin, Phys. Rev. B **80**, 134418 (2009).
[22] A. P. Malozemoff and J. C. Slonczewski, Academic Press, New York (1979).
[23] C. Phatak, A. K. Petford-Long, and M. De Graef, Curr. Opin. Solid. ST. M. **20**, 107 (2016).
[24] F. S. Yasin, L. Peng, R. Takagi, N. Kanazawa, S. Seki, Y. Tokura, and X. Yu, Adv. Mater. **32**, 2004206 (2020).
[25] K. Kurushima, K. Tanaka, H. Nakajima, M. Mochizuki, and S. Mori, J. Appl. Phys. **125**, 053902 (2019).
[26] C. L. Chien, Frank Q. Zhu, and J. G. Zhu, Phys. Today **60**, 40 (2007).